Self-assembly of diphenylalanine with preclick components as capping groups

Andrea Gemma,[1,♦] Enric Mayans,[1,2,♦] Gema Ballano,[3] Juan Torras,[1] Angélica Díaz,[1,2] Ana I. Jiménez,[3] Jordi Puiggalí,[1,2,*] Carlos Cativiela,[3,*] and Carlos Alemán[1,2,*]

[1] *Departament d'Enginyeria Química, EEBE, Universitat Politècnica de Catalunya, Edifici I.2, C/ Eduard Maristany, 10-14, 08019, Barcelona, Spain*

[2] *Research Center for Multiscale Science and Engineering, Universitat Politècnica de Catalunya, C/ Eduard Maristany, 10-14, 08019, Barcelona, Spain*

[3] *Departmento de Química Orgánica and Instituto de Síntesis Quimica y Catalisis Homogenea (ISQCH), Universidad de Zaragoza–CSIC, 50009 Zaragoza, Spain*

♦ These authors contributed equally to this work.

[*] jordi.puiggali@upc.edu, cativiela@unizar.es and carlos.aleman@upc.edu

ABSTRACT

Alkyne and azide, which are commonly used in the cycloaddition reaction recognized as "*click chemistry*", have been used as capping groups of two engineered diphenylalanine (FF) derivatives due to their capacity to form weak intermolecular interactions (*i.e.* dipole-π and π-π stacking). In Poc-FF-N_3 the alkyne and azide act as N- and C-terminal capping groups, respectively, while such positions are exchanged in N_3-FF-OPrp. The self-assembly of such two synthesized peptides have been extensively studied in their "*pre-click*" state, considering the influence of three different factors: the peptide concentration, the polarity of the medium, and the nature of the substrate. Poc-FF-N_3 assembles into microfibers that, depending on the medium and the substrate, can aggregate hierarchically in supramolecular structures with different morphologies. The most distinctive one corresponds to very stable birefringent dendritic-like microstructures, which are derived from the ordered agglomeration of microfibers. These branched supramolecular structures, which are observed in a variety of conditions, are relatively uncommon in short FF sequences. At the molecular level, Poc-FF-N_3 organizes in antiparallel β-sheets stabilized by N–H···O intermolecular hydrogen bonds and re-enforced by weak interactions between the azide and alkyne groups of neighbouring molecules. In opposition, N_3-FF-OPrp exhibits a very poor tendency to organize into structures with well-defined morphology. Theoretical calculations on model complexes indicate that the tendency of the latter peptide to organize into small amorphous agglomerates is due to its poor ability to form specific intermolecular interactions in comparison with Poc-FF-N_3. The implications of the weak interactions induced by the alkyne and azide groups, which strengthen peptide···peptide hydrogen bonds and π-ladders due to the stacked aromatic phenyl side groups, are discussed.

INTRODUCTION

In the self-assembly process, disordered molecules organize into ordered supramolecular architectures due to the synergistic combination of non-covalent forces, such as hydrogen bonding, electrostatic, π-π stacking, hydrophobic, van der Waals and dipole-dipole interactions.[1-5] As these interactions are ubiquitous in biological systems, nature has inspired artificial building blocks amenable to self-assemble into supramolecular structures.[6-9] With respect to biological building blocks, peptides are of great interest for materials science due to their structural simplicity, functional versatility, cost effectiveness, and widespread applications.[10-12]

As one of the simplest peptide building blocks, diphenylalanine (FF), a core recognition motif of Alzheimer's-amyloid polypeptide,[13] has been demonstrated to be an exciting tool for the development of new, environmental benign, functional materials. The FF peptide self-assembles into hollow nanotubes with outer diameters of 100-150 nm and micrometrical length,[13] which are thermally and chemically stable,[14,15] and exhibit excellent mechanical properties.[16] Due to these characteristics, extensive research efforts have been devoted to expand this class of peptide-based materials.[17,18] More specifically, a large number of FF-based biomaterials has been engineered considering, individually or in combination, the following general approaches: *(1)* increment the number of F residues in the peptide sequence (*i.e.* growing from FF to FFF or FFFF);[19-22] (2) add N- and/or C-terminal capping groups to the homopeptide sequence;[23-27] and (3) introduce chemical modifications at the own F residues.[28]

Among peptide capping groups, the fluorenylmethoxycarbonyl (Fmoc) has been widely studied because of its ability to form strong aromatic interactions, which frequently drive the peptide self-assembly into nanofibers or nanotubes.[17,29-32] In peptide sequences with aromatic residues, as F-homopeptides, the incorporation of the Fmoc

capping group at the N-terminus enhances the already important role played by π-π stacking interactions. Specifically, Fmoc-FF forms peptide fibrils[24] and very stable hydrogels[23,33,34] due to the π-π stacking interaction between Fmoc groups and between phenyl side groups. The ability of Fmoc aromatic moiety to facilitate gelation, which is significantly higher than that of other non-aromatic hydrophobic groups *(e.g. tert*-butoxycarbonyl), was unambiguously demonstrated studying series of functionalized dipeptides and amino acids.[35]

In a recent work we examined the self-assembly of phenylalanine-based peptides capped with Fmoc and 9-fluorenylmethyl ester (OFm) as N- and C-terminal aromatic components, respectively.[25] These systems exhibit a very high concentration of aromatic groups, which results from the complete elimination of both the normally free basic (N-terminus) and acidic (C-terminus) ends. Accordingly, supramolecular self-assembled organizations were expected to be reached through π-π stacking interactions. Polymorphic structures with stacked-braids, dendritic and microtubular morphologies were found for Fmoc-FF-OFm depending on the solvents used to promote the molecular self-assembly.[25] Furthermore, theoretical calculations on small model complexes predicted an antiparallel β-structure, which was in good agreement with FTIR spectra. The most important characteristics associated with such β-sheet disposition were: *(i)* the existence of aromatic π-ladders due to the stacked aromatic rings; and *(ii)* the formation of two strong intermolecular hydrogen bonds per pair of interacting molecules. Furthermore, the self-assembly of such highly aromatic peptides was regulated by controlling both the surface roughness and the hydrophilicity / lipophilicity of the substrate used to collect the samples.[36]

In this work, we examine the influence of the strength of intermolecular π-π stacking interactions in the self-assembly and supramolecular organization of FF-derivatives. For

this purpose, we have engineered two capped peptides with much less capacity to interact through π-π stacking than Fmoc. More specifically, the azide and alkyne, which are typically used in click-chemistry reactions (*i.e.* azide-alkyne cycloaddition) for the synthesis of molecules with different architectures and functional groups,[37-39] were chosen as terminal protecting groups. When they are in close proximity, the azide and alkyne motifs have been proved to interact through attractive non-covalent forces,[40-43] even though the resulting dipole-π and π-π interactions are apparently weaker than the π-π stacking typically found for aromatic rings. Thus, the crystal structure of compounds formed by arene rings with azide and alkyne functional groups positioned at opposite ends was found to be predominantly determined by face-to-face stacking motif of the rings.[42,43] On the other hand, Reches and coworkers[44] recently reported a series of FF-derivatives with free ends in which the azide group was introduced as a substituent in the side phenyl ring of one or the two F residues. Interestingly, the peptide substituted at the side group of the two F residues self-assembled into ordered spherical and porous structures in pure water and 1:1 methanol (MeOH) : water, whereas peptides with a single substitution did not form such ordered structures.

The chemical structure of the two peptides engineered in this work is displayed in Scheme 1. In the first one, hereafter denoted Poc-FF-N_3, the N-terminus was protected with the propargyloxycarbonyl group [Poc: –C(=O)–O–CH_2–C≡CH] while the C-terminus was blocked with the azidoethyloxi moiety (–O–CH_2–CH_2–N_3). In the second peptide, denoted N_3-FF-OPrp, the positions of alkyne and azide groups were exchanged. Thus, the N-terminus transforms into the azide group while the C-terminus was capped with the propargiloxi group (OPrp: –O–CH_2–C≡CH). The Poc-FF-N_3 and N_3-FF-OPrp assemblies, which were characterized by optical microscopy (OM) and scanning electron microscopy (SEM), have been compared with those reported for Fmoc-FF-

OFm, Fmoc-FF and FF. Moreover, in order to ascertain details about the interactions between peptide molecules, structural analyses were complemented with both spectroscopic studies and Density Functional Theory (DFT) calculations. It should be emphasized that, as our main objective was to apply the alkyne and azide moieties as weak π-interacting capping groups, the conduction of all experiments have been performed maintaining their "*preclick*" state.

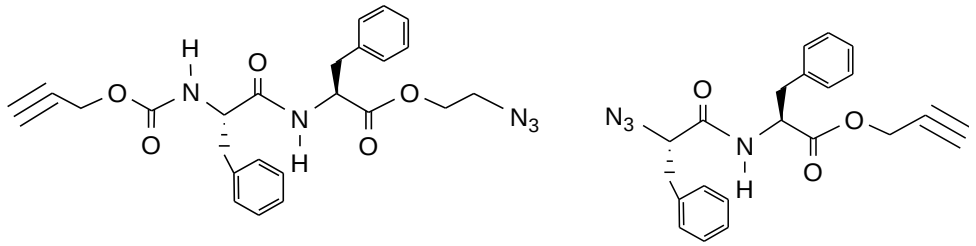

Poc-FF-N_3 N_3-FF-OPrp

Scheme 1

RESULTS AND DISCUSSION

Peptide Synthesis

The preparation of Poc-FF-N_3 and N_3-FF-OPrp was carried out following standard procedures of peptide synthesis in solution starting from the corresponding phenylalanine derivative and using the Boc, N_3 or Poc group as protection for the amino moieties. A general scheme for the coupling reactions is given in Figures 1 and 2. A detailed description of the synthetic procedure as well as the characterization of all intermediates and final peptides are supplied in the Electronic Supporting Information.

Poc-FF-N_3

Self-assembly onto glass substrates: influence of the solvents mixtures

The polymorphism of peptide assemblies is known to be concentration- and solvent-dependent.[2,7,10] The relative influence of both variables can be simultaneously investigated combining series of co-solvents with different peptide stock solutions. In this work hexafluoroisopropanol (HFIP), DCM and tetrahydrofuran (THF) peptide (5 mg/mL) stock solutions were combined with water, acetonitrile (ACN), methanol (MeOH) and isopropanol (^{i}PrOH) co-solvents. It is worth noting that the dielectric constants of these solvents (*i.e.* ε= 16.7, 8.9 and 7.6 for HFIP, DCM and THF, respectively) and co-solvents (*i.e.* ε= 78.3, 37.5, 32.6 and 17.9 for water, ACN, MeOH and ^{i}PrOH, respectively) are diverse enough to scan the effect of the medium polarity using different solvent:co-solvent mixtures with identical ratios (*i.e.* keeping constant the peptide concentration). Similarly, this strategy enables to scan the effect of the peptide concentration varying the solvent:co-solvent ratio of different mixtures (*i.e.* keeping the polarity of the medium under control).

Initially, the preservation of the peptide pre-click state in the media used in this work to promote the self-assembly, was examined by FTIR spectroscopy. Figure 3 displays the FTIR spectra of Poc-FF-N_3 and N_3-FF-OPrp samples incubated during ~1 week in representative solvent:co-solvent mixtures. The recorded spectra, which were obtained after complete evaporation of solvents mixtures in all cases, show the presence of the strong N_3 asymmetric and alkyne (RC≡CH stretching vibration) bands at 2107 and 3278 cm^{-1}, respectively, demonstrating that such environments do not promote the azide-alkyne cycloaddition reaction.

For the formation of the assembled Poc-FF-N_3 structures, 20 μL aliquots of the prepared peptide solutions were placed on microscope coverslips or glass slides (glass sample holders) and kept at room temperature (21 ºC) or inside a cold chamber (4 ºC) until dryness, no treatment being applied to accelerate the evaporation of the solvents.

The humidity was kept constant in both laboratories at 50%. In spite of the huge number of examined conditions, the structures obtained from all them were carefully examined by OM. However, SEM studies were restricted to structures that fulfilled the following requirements: *i)* to present a clearly defined morphology (*i.e.* structured morphology); *ii)* to be systematically observed when the same conditions are used in different and independent experiments (*i.e.* reproducibility); and *iii)* to remain formed upon manipulation for OM and/or SEM observations (*i.e.* stability).

From concentrated 4:1 DCM:MeOH solutions (4 g/mL), Poc-FF-N_3 was shown to form birefringent dendritic-like microstructures at room temperature (Figure 4a). Each supramolecular domain extends over hundreds of micrometres (Figure 4b) and arises from the directional grouping of fibres of nano- and micrometrical thickness, as is reflected by the high resolution SEM micrographs displayed in Figure 4c. Moreover, the hierarchic dendritic-like microstructures obtained in such conditions exhibit some morphological diversity. This is evidenced in Figure 4d, which displays OM micrographs of other birefringent dendritic-like microstructures obtained using the same experimental conditions than those used in Figure 4a. Dendritic-like structures arise systematically from DCM:MeOH solutions with peptide concentrations comprised between 4 and 2 mg/mL (*i.e.* 4:1 and 2:3 DCM:MeOH ratios), even though the density of branches rapidly decreases with the concentration (Figure 4e). Besides, Figure 4e includes high resolution SEM micrographs of the core region that nucleates the primary frameworks of the branched dendritic structure. As it can be seen, the nucleus is constituted by groups of densely staked fibres forming compact 2D aggregates. This morphology is frequently observed in the nucleus of Poc-FF-N_3 dendritic-like microstructures, independently of the peptide concentration.

Branched dendritic-like assemblies formed from HFIP:water and HFIP:EtOH mixtures have been recently reported for both Fmoc-FF-OFm and Fmoc-FFF-OFm.[25] Nevertheless, the stability of these dendritic microstructures was very poor, disappearing when the glass slip was manipulated for SEM observations. The substitution of glass slides substrates by plasma functionalized polystyrene significantly enhanced the stability of such dendritic morphologies.[36] Although the hydrophilicity of that functionalized surface precluded the massive adsorption of the aromatic peptide, the growing of branches with a 4-fold pseudo-symmetry was observed after the initial nucleation, which was the limiting step. Accordingly, repulsive peptide···surface forces in plasma functionalized polystyrene were adequately compensated by attractive peptide···peptide interactions. On the other hand, no dendritic-like structure has been described for Fmoc-FF yet, while FF requires very special experimental conditions to stabilize branched assemblies.[45,46] Thus, Tendler and co-workers[45] reported FF unstable star-like dendritic structures obtained by spin-casting a HFIP peptide solution (0.5 or 1 mg/mL) onto mica. However, such morphologies rapidly transformed into needle-like crystals upon exposure to humid air. Besides, highly ordered dendritic assemblies of FF were also achieved by Kim and co-workers,[46] who used a buffer peptide solution with pH= 1 and a silicon wafer substrate. In that case, the morphology of the self-assembled dendrites, resembled ice crystal structures in snowflakes.[47]

Dendritic-like microarchitectures obtained for Poc-FF-N_3 were expected to behave, at least partially, as fractal objects (*i.e.* self-similar structures for which increasing magnifications reveal similar features on different length scales).[48] In order to examine the extend of this behaviour, the fractal dimension (*FD*), which indicates how a fractal pattern changes with the measured scale, was determined using the box-counting method. More specifically, the binary images derived from the OM micrographs

displayed in Figures 4a and 4d, which can be considered as representative among the branched-like organization found for Poc-FF-N_3, were divided in squares boxes of side length *L* and the number of squares boxes that occupy at least part of the dendritic-like microstructure (*N*) was counted.

Figure 5, which represents logarithm plots of *N* as a function of *L*, uses the scaling relationship $N(L) \sim L^{-FD}$ to relate *FD* with slope in the logarithmic scale (*m*): $FD = -m$. Although the excellent linear behaviour displayed in Figure 5 indicates that the dendritic-like structures formed by Poc-FF-N_3 exhibit dimensional consistency at different length scales, the slopes reflect poor self-similarity. Thus, the obtained *FD* values, which range from 1.75 (Figure 4d-right) to 1.84 (Figure 4a), deviate from the ideal value of 1.67 expected for microstructures generated by diffusion limited aggregation (DLA) onto a 2D substrate surface.[49,50] Poc-FF-N_3 molecules diffuse by Brownian motion and a random walk process occurs until they contact and adhere to another one. This process gives place to the formation of clusters through attractive short-range interactions (*i.e.* hydrogen bonds and π-π stacking), which in turn interact among them forming dendritic-like microstructures. These peptide···peptide forces are weaker for Poc-FF-N_3 than for peptides with a larger F-segment (*e.g.* Fmoc-FFFF-OFm[25]). We attribute this feature not only the lower number of hydrogen bonding capability of the former but also to poor stacking ability of the alkyne and azide moieties. These features combined with the steric shielding of the internal regions of the clusters, which depends on the size of the N- and C-terminus protecting groups, are responsible of the degree of fractality of the resulting microstructures.

Replacement of the 4:1 DCM:MeOH mixture by 4:1 THF:water (*i.e.* maintaining the 4 mg/mL peptide concentration) results in a completely different microstructure. This consists in abundant, individual and birefringent microfibers with a very low degree of

branching and a "star-burst" morphology, where several microfibers are grown from a common nucleus (Figures 6a). In comparison with Figure 4, the disposition of these microfibers is very disordered. This has been attributed to the presence of a higher concentration of nuclei, as is reflected in Figure 6a (micrograph at the right side). Similarly, disordered agglomerates of relatively long microfibers (Figures 6b-c) were formed in HFIP:water at 1-2 mg/mL peptide concentrations (*i.e.* solvent:co-solvent ratios comprised between 4:1 and 2:3).

The important changes obtained in THF:water and HFIP:water with respect to DCM:MeOH solutions may be attributed to the variation of both the polarity (*i.e.* DCM:MeOH is less polar than THF:water and HFIP:water) and/or the evaporation rate (*i.e.* DCM:MeOH evaporates faster than THF:water and HFIP:water at identical experimental conditions – temperature, exposed surface area and humidity). Comparison of the results displayed in Figures 4 and 6 suggests that, in this case, the crystallization rate is mainly controlled by the polarity of the medium. Thus, considering the low polarity of the Poc-FF-N_3 molecule, peptide-peptide interactions predominate over peptide-solvent interactions in THF:water and HFIP:water increasing the concentration of nuclei, while the opposite occurs in DCM:MeOH. Accordingly, for the higher concentration of nuclei obtained in THF:water and HFIP:water, abundant and disordered microfibers are observed, while the few nuclei obtained in DCM:MeOH cause the unrestricted growth of branched supramolecular structures ideally formed for well aligned fibres.

Self-assembly from HFIP:MeOH solutions: influence of the substrate

Although the surface is known to play a noticeable control in the self-assembly of compounds,[36,45,51-53] studies about the influence of solid substrate on the assembly of F-

derivatives are relatively scarce. More specifically, this phenomenon has been only reported for the parent FF dipeptide[45,51] and the highly aromatic Fmoc-FFF-OFm.[36] In this sub-section, we examine the surface mediated hierarchical assembly of Poc-FF-N_3 from HFIP:MeOH solutions considering glass, silanized glass, plasma-functionalized polystyrene and stainless steel AISI 316.

Glass promotes the formation of well-defined microfibers (Figure 7a), which are aggregated to a lesser extent than those formed in HFIP:MeOH (Figures 6c-d). In silanized glass the mineral surface is treated with Cl_2SiMe_2 to increase its hydrophobicity (*i.e.* the contact angle increases from 58º±2º to 76º±2º) without alter the very low surface roughness (*i.e.* 1.5±0.5 and 3.5±0.8 nm for glass and silanized glass, respectively). Drop-cast of Poc-FF-N_3 solutions in HFIP:MeOH onto silanized resulted in the formation of micro- and nanofibers that hierarchically aggregate in reproducible doughnut-like supramolecular structures like those displayed in Figures 7b and S1. Although the size of such rounded-like supramolecular structures increases with the peptide concentration (Figure S1), they are relatively isolated. Thus, for low concentrations the peptide is not observed in large areas of the surface, as is illustrated in Figures S1b-c, suggesting that fibre⋯fibre interactions predominate over fibre⋯surface ones. Deposition of the peptide dissolved onto steel AISI 316 results in the spontaneous formation of similar hollow rounded-like supramolecular structures (Figure 7c). This should be attributed to the fact that the properties of the latter substrate (*i.e.* contact angle and roughness of 74º±7º and 14.4±3.2 Å, respectively) and silanized glass are very similar.

Plasma-treatment of polystyrene is the method of choice for routinely incorporate oxygen-containing moieties in bioactive polystyrene surfaces to increase their hydrophilicity and promote cell-polymer interactions.[54] The morphology of the

assemblies formed in this substrate, which is the most hydrophilic of those examined (*i.e.* contact angle and roughness of 41º±2º and 8.5±4.5 Å, respectively), exhibit a great dependence on the peptide concentration. Thus, dense and disordered fibre agglomerates (Figure S2a) are derived from concentrated peptide solutions, whereas low peptide concentrations (0.5-0.1 mg/mL) systematically promote the formation of dendritic-like structures (Figures 7d and S2b). The latter resemble the long branched morphologies observed when concentrated Poc-FF-N_3 DCM:MeOH solutions are casted onto a glass substrate. Low and high resolution SEM micrographs (Figure 7e) reflect that such dense branched architectures result from the hierarchical agglomeration of microfibers, which in turns are constituted by precisely aligned groups of nanometric fibres.

Long (several micrometres) and uniform nano- and microfibers are frequently assembled from F-homopeptides possessing a large variety of blocking groups because of their ability to form hydrogen bonds and π-π stacking interactions.[13-27] However, because of the small size, regular chemical architectures and lack of branching of these molecules, they are not expected to form supramolecular dendritic-like structures on a large scale. In spite of this, we recently found that Fmoc-FFFF-OFm self-assembles into very stable dendritic microarchitectures made of branches growing from nucleated primary frameworks since peripheral π-π stacking interactions promoted branched architectures.[25] However, in the case of Poc-FF-N_3, SEM and OM micrographs suggest a mechanism based on the formation of a few nucleation centres on the glass and polystyrene surfaces. These nuclei favour the growth of uniformly oriented microfibers, which are probably stabilized through specific hydrogen bonds.

The internal structure of these fibres is expected to differ from those obtained for uncapped FF,[13,55] which are formed by cyclic aggregates of four molecules stabilized by

head-to-tail hydrogen bonds. The cycles stack in sheets forming hydrophobic tubes that, in turn, self-associate forming fibres. For Poc-FF-N_3 fibres we hypothesize the formation of alkyne···azide interactions, which have been observed in both aromatic organic compounds and biomolecules blocked with azide and alkyl groups,[56-59] and the the participation of stronger intermolecular interactions involving the peptide and/or phenyl groups. The structure of both the sheets and the tubes has been examined in the next sub-section.

Table 1 compares the different supramolecular structures observed for Poc-FF-N_3 under different experimental conditions.

Structure of the sheets and intermolecular interactions

FTIR spectroscopy has revealed that the presence of β-sheets can be determined by analysing the amide I bands, which occur in the wavenumber range from 1600 cm^{-1} to 1700 cm^{-1}, and arise primarily from stretching vibrations of main chain carbonyl groups. Early investigations suggested that FTIR spectroscopy might be able to distinguish between parallel and antiparallel β-sheets.[60-63]

Figure 3a displays the amide I regions of the FTIR spectra recorded for the structures derived from 4 and 1 mg/mL Poc-FF-N_3 solutions in DCM:MeOH and HFIP:water, respectively. The spectra, which were recorded for peptide structures formed after solvent evaporation, show two bands in the amide I region. The most intense band appears at 1655 cm^{-1}, while the least intense one is at 1699 cm^{-1}. This feature is consistent with an antiparallel disposition of the β-sheets. However, the 1699 / 1650 ratio is below one (*i.e.* around 0.75), suggesting that the percentage of antiparallel arrangement is relatively low. On the other hand, the fact that the major component appears in all cases, independently of the solvent mixture and peptide concentration, at

the same position (1655 cm^{-1}) indicates the absence of excitonic coupling effects in the frequency position.[64] On the other hand, the amide II and C=O stretching bands appear at 1541 and 1734 cm^{-1}, respectively, while the amide A at around 3310 cm^{-1} partially overlaps the alkyne band at 3278 cm^{-1}.

In order to obtain information about the structure of the aggregates in the first stages of the assembly process, circular dichroism (CD) spectra were recorded at very low peptide concentration (0.01 mg/mL) in different environments (*i.e.* 1:9 DCM:MeOH, HFIP:water, HFIP:MeOH and HFIP:^{i}PrOH mixtures coming from 1 mg/mL DCM or HFIP stock solutions). The CD spectra recorded at 30 ºC for the different mixtures are compared in Figure 8a. In HFIP:MeOH, Poc-FF-N_3 molecules are predominantly in random coil conformation, which is proved by the negative band at 196 nm. In contrast, the spectrum obtained in DCM:MeOH, which exhibits a positive band at 197 nm and a negative band at 208 nm, suggests the dominance of a β-sheet structure. The positive maxima at around 200 and 220 nm indicate the presence of π-π stacking of aromatic units in dilute HFIP:water and HFIP:^{i}PrOH solutions. This interaction is frequently detected in the CD profiles for biomolecular self-assembly with β-turn conformation.[65,66] In all cases these structural characteristics are preserved between -50 ºC and +60 ºC, as is demonstrated by the spectra acquired at different temperatures within such interval (Figure S3).

Density functional theory (DFT) calculations were carried out considering different structural models. First, the relative stability of the antiparallel and parallel β-sheet dispositions was examined using mode complexes involving three β-strands. In an attempt to optimize the geometry of the inter-strand interactions (*i.e.* hydrogen bonds and π-π stacking), different starting arrangements were constructed for each disposition. Geometry optimizations were performed using the M06L, M06L-D3 and BLYP-D3

correlated functionals combined with the 6-31G(d) basis set. Results indicated that the antiparallel disposition is the most stable, independently of the computational method, which is agreement with the FTIR observations. Table 2, which lists the relative energies (ΔE) obtained using the different theoretical levels, indicates that the parallel disposition was disfavoured by around 0.9-3.7 kcal/mol, depending on the functional.

The antiparallel disposition was proposed by Smith *et al.*[31] for Fmoc-FF and by Mayans *et al.*[25] for Fmoc-FF-OFm. Comparison of the models reported for the parallel and antiparallel β-sheets of such Fmoc-containing dipeptides reveals that intermolecular interactions are characterized by the following trends:

(i) In the parallel disposition the phenyl side groups of all strands are perfectly packed forming aromatic π-ladders, while the phenyl groups of consecutive strands point in opposite directions in the antiparallel arrangement.

(ii) Fmoc-FF-OFm exhibits similar Fmoc···Fmoc interactions for both the parallel and antiparallel dispositions, whereas in the case of Fmoc-FF such interactions are much stronger for the parallel assembly than for the antiparallel one.

(iii) Hydrogen bonding parameters, especially the H···O distance, are more favourable for the antiparallel than for the parallel assembly.

These features reflect the predominant role played by hydrogen bonds in the packing of Fmoc-containing FF-derivatives. Results from the analysis of the intermolecular interactions in the antiparallel and parallel dispositions modelled for Poc-FF-N_3 β-strands, which are displayed in Figures 9a-b and S4, are compared in Table 2. As it can be seen in Figures 9b, S4b and S4d (for geometries optimized at the B3LYP-D3/6-31G(d), M06L-D3/6-31G(d) and M06L/6-31G(d) level, respectively), the parallel

disposition of Poc-FF-N_3 molecules shows the same alignment of the phenyl side groups reported for Fmoc-FF-OFm.[25] This attractive interaction, which originates the formation of aromatic π-ladders, is practically absent in the antiparallel disposition (Figures 9a, S4a and S4c). On the other hand, hydrogen bonding parameters also favour the parallel disposition in comparison with the antiparallel one (Table 2). The stability of the antiparallel disposition with respect to the parallel is explained by comparing the alkyne···azide interactions detected for the former with the azide···azide and alkyne···alkyne interactions of the latter. Thus, although the distances between the π-π stacked groups are, in general, slightly shorter for the parallel disposition than for the antiparallel one (Table 2), π-dipole interactions are only possible for the former arrangement (Figures 9a, S4a and S4c). According to these DFT calculations and the FTIR spectra, π-dipole interactions play a crucial role in the assembly of Poc-FF-N_3 molecules, which is fully consistent with the crystal X-ray analyses of compounds containing azide and alkyne motifs.[40-43] Thus, in such compounds the azide and alkyne groups of adjacent molecules are arranged in a head-to-tail fashion, which is equivalent to the antiparallel disposition of Poc-FF-N_3 strands, favouring the formation of dipole-π interactions in addition of π-π interactions.

On the other hand, by analogy with the structures reported for FF[55] and FFFF[22] nanotubes, cycles of dimers, trimers and tetramers (*i.e.* 2, 3 and 4 Poc-FF-N_3 molecules disposed forming a ring with a central channel) were constructed. Thus, the stacking and lateral packing of such cycles should result in the growing of fibres. In the starting cyclic complexes, the alkyne and azide groups of neighbouring peptide molecules were arranged to form head-to-tail π-π stacking interactions, which surrounded the inner core of the rings, while phenyl side chains emanated from the rings forming the hydrophobic external side. Geometry optimizations at the M06L/6-31G(d) level led to the minimum

structures displayed in Figure 10. As it can be seen, complexes with molecules arranged in irregular dispositions were obtained in all cases, even though the disorganization of the molecules increases with the size of the complex. The formation during the optimization of both N–H···O hydrogen bonds (*i.e.* complexes with 3 and 4 molecules; Figures 10b-c) and N-H···π interactions (*i.e.* complex with 4 molecules; Figure 109c), explains the loss of the starting cyclic disposition. Thus, the strength of hydrogen bonds is significantly higher than that of alkyne···azide head-to-tail interactions. Therefore, hydrogen bonds governed the re-organization of the molecules in the complexes, inducing the loss of the starting cyclic geometries during the optimization. This fact explains that Poc-FF-N_3 fibres are much less defined and ordered than the FF fibers, which adopt a hexagonal-like shape due to the high stability of the head-to-tail $NH_3^+\cdots^-$OOC hydrogen bonds in FF cyclic hexamers.[55]

N_3-FF-OPrp

The "*preclick*" state of the peptide after evaporation of the solvent is corroborated in the FTIR spectra displayed in Figure 3b. The strong N_3 asymmetric band appears at 2113 cm^{-1}, while the alkyne stretching is contained in the broad band centred at 3296 cm^{-1}, which also includes the amide A vibration. Also, some bands attributed to trapped solvent molecules are observed in the region of 2350 cm^{-1}.

The experimental conditions (*i.e.* solvent:co-solvent mixtures and substrates) used in the previous section for Poc-FF-N_3, were applied to explore the assembly behaviour of N_3-FF-OPrp. Amazingly, after many attempts at room temperature, we concluded that the latter peptide hardly forms nano- or microstructures with well-defined morphologies. Thus, N_3-FF-OPrp tends to organize into small amorphous agglomerates completely irregular or with short-range regularity, independently of the experimental

conditions at room temperature. This is illustrated in Figure S5, which displays representative micrographs of the disordered assemblies obtained using different solvent:co-solvents and substrates.

In order to expand this search of regular N_3-FF-OPrp assemblies, new sets of experiments were performed keeping the samples inside a cold chamber (4 ºC) during the solvent drying process. In this case, an exception to the general behaviour observed for N_3-FF-OPrp was obtained for diluted (< 1 mg/mL) HFIP:water solutions deposited onto glass coverslips, which systematically resulted in the formation regular assemblies, as it is reflected in Figure 11. In such particular experimental conditions the peptide forms well-defined spheres of heterogeneous sizes (*i.e.* the diameter ranged from ~20 to ~200 nm), which in turn aggregate forming micrometric structures with a honeycomb morphology. This behaviour has been attributed to the hydrophobicity of the N_3-FF-OPrp, which forces the refolding of the structures to protect many molecules from the aqueous medium. Thus, the initial organization of the peptide in nanospheres and their subsequent aggregation in microstructures are consequence of the repulsive interaction with the polar environment (*i.e.* diluted peptide HFIP:water solutions present a high content of co-solvent).

CD spectra of 0.01 mg/mL N_3-FF-OPrp solutions in 1:9 DCM:MeOH, HFIP:water, HFIP:MeOH and HFIP:^{i}PrOH mixtures are shown in Figure 8b. In HFIP:MeOH and, especially, HFIP:^{i}PrOH the spectra are appreciably contributed by the random coil conformation, as is evidenced by the negative band at 197-198 nm. Besides, the spectra obtained in DCM:MeOH and HFIP:water do not suggest any conformational preference. These results, which are independent of the temperature (Figure S6), support that N_3-FF-OPrp agglomerates start from small aggregates of unstructured peptide molecules.

The amide I band of the FTIR spectra recorded for N_3-FF-OPrp aggregates after evaporation of the solvent (Figure 3b) reflects important changes in comparison to those obtained for Poc-FF-N_3 (Figure 3a). More specifically, the two narrow and strong peaks observed for the latter at 1655 and 1699 cm^{-1} transforms into a single and relatively broad peak centred at 1678 cm^{-1}. The position of this band is relatively far from that typically observed for parallel β-sheets (*i.e.* ~1650 cm^{-1}).-This feature suggests that the N_3-FF-OPrp molecules tend to poorly organize in distorted or irregular parallel sheets. These results was supported by B3LYP-D3/6-31G(d) calculations on complexes formed by three or five molecules arranged in antiparallel and parallel β-sheets (Figures S7 and 12).

Geometry optimizations of the antiparallel β-sheet resulted in the formation of unstructured complexes (Figures S7a and 12a), in which characteristic alignment of the molecules is lost. Moreover, comparison of the geometries obtained for complexes with three and five N_3-FF-OPrp strands evidence that the stability of the antiparallel β-sheet does not increase with the number of interacting molecules. On the other hand, the parallel disposition, which is energetically favoured with respect to the antiparallel one (*i.e.* 8.1 and 13.9 kcal/mol for complexes with 3 and 5 N_3-FF-OPrp molecules, respectively), preserves the β-sheet structure (Figures S7b and 12b). These results are explained by examining the capacity of N_3-FF-OPrp to form intermolecular interactions. Thus, due to the single peptide bond of its chemical structure (Scheme 1), each N_3-FF-OPrp molecule only participates in two intermolecular hydrogen bonds: one as acceptor and one as donor. This represents a significant reduction with respect to Poc-FF-N_3 (Figures 9a and S4), in which peptide molecules used their two peptide bonds to interact forming four hydrogen bonds per molecule (*i.e.* two as acceptor and two as donor). Accordingly, the possible formation of two hydrogen bonds per N_3-FF-OPrp molecule

is not enough to stabilize the antiparallel β-sheet disposition, which disrupts and gives place to a disordered aggregation of molecules. In the case of the parallel β-sheet disposition, the two hydrogen bonds are strengthened by the existence of aromatic π-ladders formed by stacked phenyl rings. Interactions between aromatic rings, which are not possible in the antiparallel disposition, are more stabilizing than alkyne···azide interactions,[40-43] explaining the cohesion of the parallel disposition and the unsteadiness of the antiparallel one.

On the other hand, alkyne···alkyne are the only π-π interactions detected in the parallel model of N_3-FF-OPrp, the distance between the azide groups of adjacent molecules (> 5 Å in all cases) hampering the formation of azide···azide interactions. This has been attributed to the fact that rest of interactions found in such organization determine the molecular conformation because of their higher strength. Overall, the distortions and irregularities suggested by FTIR in the β-sheets of N_3-FF-OPrp can been attributed to the relatively poor interaction pattern of the latter compound with respect to that of Poc-FF-N_3.

CONCLUSIONS

We have successfully synthesized and study the self-assembly of FF-derivatives capped at the N- and C-terminus by azide and alkyne groups, which have been maintained in the *preclick* state. Results prove that despite intermolecular azide···alkyne interactions are significantly weaker than hydrogen bonding in FF and Fmoc···Fmoc π-π interactions in Fmoc-FF-OFm, Poc-FF-N_3 molecules hierarchically aggregate forming well-defined supramolecular structures. Furthermore, the morphology of such structures can be regulated through the peptide concentration, the polarity of the medium and/or the hydrophilicity of substrate. In particular, the formation of stable dendritic-like

structures is very striking since, although this kind of branched structures was recently detected in homopeptides with a higher number of phenylalanine residues, they were found to be highly unstable for other FF-derivatives (*e.g.* Fmoc-FF-Fmoc[25]). Theoretical calculations and FTIR spectra probe that Poc-FF-N_3 assemblies prefer antiparallel β-sheets. This has been attributed to the strength of azide⋯alkyne interactions, which exhibit two components: π-π stacking and π-dipole. The sum of these contributions is more stabilizing than the π-π stacking of the azide⋯azide and alkyne⋯alkyne interactions found in the parallel β-sheet.

The similar peptide in which the position of the alkyne and azide groups was exchanged, N_3-FF-OPrp, exhibited much less tendency to form ordered structures under the same experimental conditions. Indeed, the only supramolecular assembly identified for N_3-FF-OPrp was observed in very polar environments, in which peptide molecules organize in nanospheres that subsequently aggregate into honeycomb supramolecular structures. Furthermore, the parallel is the only stable β-sheet disposition found for this peptide, molecules arranged in the antiparallel disposition evolving towards completely disordered structures during geometry optimizations. The assembly of N_3-FF-OPrp molecules is governed by the formation of phenyl π-ladders due to their restricted hydrogen bonding capacity. Overall, results obtained in this work reflect that, although the role of the interactions involving alkyne and azide groups is much less decisive than the one played by hydrogen bonds and aromatic π-π stacking interactions, the formers allow modulation of the assembly stabilizing microstructures that are usually unstable.

ACKNOWLEDGEMENTS

Authors thank supports from MINECO and FEDER (MAT2015-69367-R, MAT2015-69547-R and CTQ2013-40855-R) and Gobierno de Aragón - FEDER

(research group E40). Support for the research of C.A. was received through the prize "ICREA Academia" for excellence in research funded by the Generalitat de Catalunya.

REFERENCES

1. A. Ciesielski, M. El-Garah, S. Masiero and P. Samori,*Small*, 2016, **12**, 83-95.
2. C. H. Cai, J. P. Lin, Y. Q. Lu, Q. Zhang and L. Q. Wang, *Chem. Soc. Rev.*, 2016, **45**, 5985-6012.
3. Y. Liu, B. Liua and Z. Nie, *Nano Today*, 2015, **10**, 278-300.
4. A. Groschel and A. H. E. Mueller, *Nanoscal*e, 2015, **7**, 11841-11876.
5. S. Scanna, D. J. Pine and G.-R. Yi, *Soft Matter*, 2013, **9**, 8096-8106.
6. L. Z. Zhao, R. Qu, A. Li, R. J. Ma and L. Q. Shi, *Chem. Commun.*, 2016, **52**, 13543-13555.
7. G. Fichman and E. Gazit, *Acta Biomater.*, 2014, **10**, 1671-1682.
8. Y. Zhao, F. Sakai, L. Su, Y. J. Liu, K. C. Wei, G. S. Chen and M. Jiang, *Adv. Mater*., 2013, **25**, 5215-5256.
9. K. H. Smith, E. Tejeda-Montes, M. Poch and A. Mata, *Chem. Soc. Rev.*, 2011, **40**, 4563-4577.
10. K. Tao, A. Levin, L. Adler-Abramovich and E. Gazit, *Chem. Soc. Rev.*, 2016, **45**, 3935-3953.
11. B. E. I. Ramakers, J. C. M. van Hest and D. W. P. M. Lowik, *Chem. Soc. Rev.*, 2014, **43**, 2743-2756.
12. Peptide Materials: From Nanostructures to applications, C. Alemán, A. Bianco and M. Venanzi (Eds), Wiley, 2013.
13. M. Reches and E. Gazit, *Science*, 2003, **300**, 625-627.

14. V. L. Sedman, L. Adler-Abramovich, S. Allen, E. Gazit and S. J. B. Tendler, *J. Am. Chem. Soc.*, 2006, **128**, 6903-6908.
15. L. Adler-Abramovich, M. Reches, V. L. Sedman, S. Allen and S. J. B. Tendler, *Langmuir*, 2006, **22**, 1313-1320.
16. N. Kol, L. Adler-Abramovich, D. Barlam, R. Z. Shneck, E. Gazit and I. Rousso, *Nano Lett.*, 2005, **5**, 1343-1346.
17. X. Yan, P. Zhu and J. Li, *Chem. Soc. Rev.*, 2010, **39**, 1877-1890.
18. S. Fleming and R. V. Ulijn, *Chem. Soc. Rev.*, 2014, **43**, 8150-8177.
19. P. Tamamis, L. Adler-Abramovich, M. Reches, K. Marshall, P. Sikorski, L. Serpell, E. Gazit and G. Archontis, *Biophys. J.*, 2009, **96**, 5020-5029.
20. C. Guo, Z. A. Arnon, R. Qi, Q. Zhang, L. Adler-Abramovich, E. Gazit and G. Wei, *ACS Nano*, 2016, **10**, 8316-8324.
21. C. Guo, Y. Luo, R. Zhou and G. Wei, *Nanoscale*, 2014, **6**, 2800-2811.
22. E. Mayans, G. Ballano, J. Casanovas, A. Díaz, M. M. Pérez-Madrigal, F. Estrany, J. Puiggalí, C. Cativiela and C. Alemán, *Chem. Eur. J.*, 2015, **21**, 16895-16905.
23. V. Jayawarna, M. Ali, T. A. Jowitt, A. F. Miller, A. Saiani, J. E. Gough and R. V. Ulijn, *Adv. Mater.*, 2006, **18**, 611-614.
24. N. Amdursky, E. Gazit and G. Rosenman, *Adv. Mater.*, 2010, **22**, 2311-2315.
25. E. Mayans, G. Ballano, J. Casanovas, L. J. del Valle, M. M. Pérez-Madrigal, F. Estrany, A. I. Jiménez, J. Puiggalí, C. Cativiela and C. Alemán, C, *Soft Matter*, 2016, **12**, 5475-5488.
26. N. Amdursky, M. Molotskii, E. Gazit and G. Rosenman, *Appl. Phys. Lett.*, 2009, **94**, 261907.
27. L. Adler-Abramovich, N. Kol, I. Yanai, D. Barlam, R. Z. Shneck, E. Gazit and I. Rousso, *Angew. Chem. Int. Ed.*, 2010, **49**, 9939-9942.

28. M. Reches and E. Gazit, *Phys. Biol.* 2006, **3**, S10-S19.

29. S. Flemming and R. V. Ulijn, *Chem. Soc. Rev.*, 2014, **43**, 8150-8177.

30. S. Bai, C. Pappas, S. Debnath, P. W. J. M. Frederix, J. Leckie, S. Fleming and R. V. Ulijn, *ACS Nano*, 2014, **8**, 7005-7013.

31. A. M. Smith, R. J. Williams, C. Tang, P. Coppo, R. F. Collins, M. L. Turner, A. Saiani and R. V. Ulijn, *Adv. Mater.*, 2008, **20**, 37-41.

32. A. K. Das, R. Collins and R. V. Ulijn, *Small*, 2008, **4**, 279-287.

33. A. Mahler, M. Reches, M. Rechter, S. Cohen and E. Gazit, *Adv. Mater.*, 2006, **18**, 1365-1370.

34. J. Raeburn, C. Mendoza-Cuenca, B. N. Cattoz, M. A. Little, A. E. Terry, A. Z. Cardoso, P. C. Griffiths and D. J. Adams, *Soft Matter*, 2015, **11**, 927-935.

35. S. Debnath, A. Shome, D. Das and P. K. Das, *J. Phys. Chem. B*, 2010, **114**, 4407-4415.

36. E. Mayans, G. Fabregat, R. Juárez, C. Cativiela, J. Puiggalí and C. Alemán, *Chem. Select*, 2017, **22**, 1133-1139.

37. F. Amblard, J. H. Cho and R. F. Schinazi, *Chem. Rev.*, 2009, **109**, 4207-4220.

38. P. L. Golas and K. Matyjaszewski, *Chem. Soc. Rev.*, 2010, **39**, 1338-1354.

39. W. Tang and M. L. Becker, *Chem. Soc. Rev.*, 2014, **43**, 7013-7039.

40. A. Pathigoolla, R. G. Gonnade and K. M. Sureshan, *Angew. Chem. Int. Ed.*, 2012, **51**, 4362-4366.

41. W. Li, X. Li, W. Zhu, C. Li, D. Xu, Y. Ju and G. Li, *Chem. Commun.*, 2011, **47**, 7728-7730.

42. .B.-B. Ni, C. Wang, H. Wu, J. Pei and Y. Ma, *Chem. Commun.*, 2010, **46**, 782–784.

43. A. Pathigoolla and K. M. Sureshan, *Angew. Chem. Int. Ed.*, 2014, **53**, 9522-9525.

44. S. Yuran, Y. Razvag, P. Das and M. Reches, *J. Pept. Sci.*, 2014, **20**, 479-486.

45. V. V. Korolkov, S. Allen, C. J. Roberts and S. J. B. Tendler, *Faraday Discuss.*, 2013, **166**, 257-267.

46. T. H. Han, J. K. Oh, G.-J. Lee, S. II Pyun and S. O. Kim, *Colloids Surf. B*, 2010, **79**, 440-445.

47. L. Chronopoulou, S. Sennato, F. Bordi, D. Giannella, A. Di Nitto, A. Barbetta, M. Dentini, A. R. Togna, G. I. Togna, S. Moschini and C. Palocci, *Soft Matter*, 2014, **10**, 1944-1952.

48. B. B. Mandelbrot, *The Fractal Geometry of Nature*, Freeman, San Francisco, CA, USA, 1982.

49. T. A. Witten and L. M. Sander, *Phys. Rev. Lett.*, 1981, **47**, 1400-1403.

50. P. Meakin, *Phys. Rev. A*, 1983, **27**, 604-607.

51. P. Kumaraswamy, R. Lakshmanan, S. Sethuraman and U. M. Krishnan, *Soft Matter*, 2011, **7**, 2744-2754.

52. L. Klosterman, J. K. Riley, C. J. Bettinger, *Langmuir*, 2015, **31**, 3451-3458.

53. X. B. Mao, C. X. Wang, X. K. Wu, X. J. Ma, L. Liu, L. Zhang, L. Niu, Y. Y. Guo, . H. Li, Y L. Yang and C. Wang. *Proc. Natl. Acad. Sci. USA*, 2011, **108**, 19605-19610.

54. T. G. van Kooten, H. T. Spijker and H. J. Busscher, *Biomaterials*, 2004, **25**, 1735-1747.

55. C. H. Görbitz, *Chem. Eur. J.*, 2001, **7**, 5153-5159.

56. B.-B. Ni, C. Wang, H. Wu, J. Pei and Y. Ma, *Chem. Commun.*, 2010, **46**, 782–784.

57. T. Hirose, N. Maita, H. Gouda, J. Koseki, T. Yamamoto, A. Sugarawa, H. Nakano, S. Hirono, K. Shiomi, T. Watanable, H. Taniguchi, K. B. Sharpless, S. Omura and T. Sunazuka, *Proc. Natl. Acad. Sci.*, 2013, **110**, 15892–15897.

58. A. Pathigoolla and K. M. Sureshan, *Angew. Chem. Int. Ed.*, 2014, **53**, 9522-9525.

59. A. Pathigoolla and K. M. Sureshan, Chem.Commun., 2016, **52**, 886-888.

60. C. Toniolo and M. Palumbo, *Biopolymers*, 1977, **16**, 219-224.

61. S. Krimm and J. Bandekar, *Adv. Protein Chem.*, 1986, **38**, 181-364.

62. R. Khurana and A. L. Fink, *Biophys. J.*, 2000, **78**, 994-1000.

63. E. Goormaghtigh, V. Cabiaux and J.-M. Ruysschaert, *Subcell. Biochem.*, 1994, **23**, 329-362.

64. L. Z. Polzi, A. Amadei, M. Aschi and I. Daidone, *J. Am. Chem. Soc.*, 2011, **133**, 11414-11417.

65. M. Gupta, A. Bagaria, A. Mishra, P. Mathur, A. Basu, S. Ramakumar and V. S. Chauhan, *Adv. Mater.*, 2007, **19**, 858-861

66. X. Yan, Y. Cui, Q. He, K. Wang and J. Li, *Chem. Mater.*, 2008, **20**, 1522-1526.

CAPTIONS TO FIGURES

Figure 1. Scheme of the coupling reactions used to obtain Poc-FF-N_3. *i)* Boc-L-Phe-OH, *N*-[3-(dimethylamino)-propyl]-*N*'-ethylcarbodiimide hydrochloride (EDC·HCl)/1-hydroxy-7-azabenzotriazole (HOBt), 2-bromoethanol, 4-dimethylaminopyridine (DMAP), DCM. *ii*) NaN_3, DMF. *iii)* H-L-Phe-OH, $NaHCO_3$ 1N (aqueous), NaOH 4N (aqueous), propargyl chloroformate. *iv)* TFA/DCM 1/1. *v)* Poc-L-Phe-OH, *N*-[3-(dimethylamino)-propyl]-*N*'-ethylcarbodiimide hydrochloride (EDC·HCl)/1-hydroxy-7-azabenzotriazole (HOBt), *N*-methylmorpholine (NMM; to keep pH 8), DCM.

Figure 2. Scheme of the coupling reactions used to obtain N_3-FF-Prp. *i)* Boc-L-Phe-OH, *N*-[3-(dimethylamino)-propyl]-*N*'-ethylcarbodiimide hydrochloride (EDC·HCl)/1-hydroxy-7-azabenzotriazole (HOBt), propargyl alcohol, 4-dimethylaminopyridine (DMAP), DCM. *ii)* H-L-Phe-OH, triethylamine (NEt_3), 1*H*-benzotriazole-1-sulfonyl azide, $CuSO_4 \cdot 5H_2O$, MeCN/H_2O (1/1). *iii)* TFA/DCM 1/1. *iv)* N_3-L-Phe-OH, *N*-[3-(dimethylamino)-propyl]-*N*'-ethylcarbodiimide hydrochloride (EDC·HCl)/1-hydroxy-7-azabenzotriazole (HOBt), *N*-methylmorpholine (NMM; to keep pH 8), DCM.

Figure 3. FTIR spectra of (a) Poc-FF-N_3 and (b) N_3-FF-OPrp samples from 4:1 DCM:MeOH and 1:4 HFIP:water solutions (4 and 1 mg/mL peptide concentration, respectively).

Figure 4. Microstructures obtained by self-assembly from Poc-FF-N_3 solutions in DCM:MeOH mixtures at room temperature. (a,b) OM micrographs of representative birefringent dendritic-like structures derived from 4 mg/mL peptide solutions (4:1 DCM:MeOH). (c) High resolution SEM micrographs of fibres hierarchically aligned to form the dendritic-like structures displayed in (a) and (b). (d) OM micrographs of other frequently observed birefringent dendritic-like morphologies derived from 4 mg/mL peptide solutions. (e) OM micrographs (left) of representative birefringent dendritic-like

structures derived from 2 mg/mL peptide solutions (2:3 DCM:MeOH) and high resolution SEM micrographs (centre and right) of the nucleus, which is indicated by the red dashed rectangle in the left micrograph. Micrographs displayed at the right show details of the region marked by the red dashed circle.

Figure 5. Analysis of the fractal dimension using the box-counting method for the Poc-FF-N_3 dendritic-like microstructures displayed in Figures 4a and 4d (both left and right). The fractal dimension is related to the slope of the adjusted equations (see text).

Figure 6. (a) Disordered birefringent microfibers obtained from 4 mg/mL Poc-FF-N_3 solutions in 4:1 THF:water. Disordered agglomerates of microfibers formed from (b) 1 and (c) 2 mg/mL Poc-FF-N_3 solutions in 1:4 and 2:3 HFIP:water, respectively.

Figure 7. Optical and/or SEM representative micrographs of Poc-FF-N_3 assemblies formed onto (a) glass coverslip, (b) silanized glass, (c) steel AISI 316 and (d-e) plasma treated polystyrene using (a) 0.5 mg/mL (1:9), (b) 0.1 mg/mL (1:49), (c) 4 mg/mL (4:1), (d-e) 0.5 mg/mL (1:9) HFIP:MeOH solutions (solvent:co-solvent ratio indicated in parenthesis).

Figure 8. CD spectra of (a) Poc-FF-N_3 and (b) N_3-FF-OPrp in different environments (1:9 solvent:co-solvent) at 0.01 mg/mL peptide concentration.

Figure 9. Lateral and top views of the (a) antiparallel and the (b) parallel β-sheet assemblies obtained for a complex with three Poc-FF-N_3 strands. Geometries were optimized at the B3LYP-D3/6-31G(d) level. Intermolecular hydrogen bonds are represented by black dashed lines, the (N–)H···O distances (in Å) being displayed. Intermolecular azide···alkyne, azide···azide, and alkyne···alkyne interactions are represented by pink dashed lines. These three π-stacking interactions have been considered to occur when the distance between the two motifs is lower than 4.5 Å (values are provided in the graphic). Azide···alkyne distances in the antiparallel

disposition, have been determined considering the central nitrogen atom of the azide group and each of the two carbons of the alkyne group. Azide···azide and alkyne···alkyne distances in the parallel disposition have been determined considering the central nitrogen atom of each azide group and the geometric centre of each C≡C bond, respectively.

Figure 10. Lateral and top views of complexes formed by (a) two, (b) three and (c) four Poc-FF-N_3 molecules after geometry optimization at the B3LYP-D3/6-31G(d) level. In all cases molecules were initially arranged forming cycles with alkyne···azide head-to-tail interactions. Intermolecular hydrogen bonds are represented by black dashed lines, the (N–)H···O distances (in Å) being displayed. Intermolecular alkyne···azide interactions are represented by pink dashed lines. The latter interaction has been considered to occur when the distance between the two motifs is lower than 4.5 Å (values are provided in the graphic).

Figure 11. Representative optical and/or SEM micrographs of N_3-FF-OPrp assemblies formed at 4 ºC onto glass coverslips using a 0.5 mg/mL peptide solution in1:9 HFIP:water.

Figure 12. Lateral and top views of the geometries obtained after optimization of the (a) antiparallel and the (b) parallel β-sheet assemblies constructed using five N_3-FF-OPrp strands. Geometries were optimized at the B3LYP-D3/6-31G(d) level. Intermolecular hydrogen bonds are represented by black dashed lines, the (N–)H···O distances (in Å) being displayed. Intermolecular alkyne···alkyne interactions are represented by pink dashed lines. These interactions have been considered to occur when the distance between the geometric centre of two adjacent alkyne motifs is lower than 4.5 Å (values are provided in the graphic). Azide···azide distances were larger than 5 Å.

Table 1. Summary of the self-assemblies observed in this work for Poc-FF-N_3 and N_3-FF-OPrp. The experimental conditions are provided in each case.

Solvent mixture	Peptide concentration	Temperature	Substrate	Self-assembly
			Poc-FF-N_3	
4:1-2:3 DCM:MeOH	2-4 mg/mL	25 ºC	Glass coverslip	Birefringent dendritic-like microstructures
4:1 THF:water	4 mg/mL	25 ºC	Glass coverslip	Birefringent microfibers with "star-burst" morphology
4:1-2:3 HFIP:water	1-2 mg/mL	25 ºC	Glass coverslip	Agglomerates of long microfibers
1:9 HFIP:MeOH	0.5 mg/mL	25 ºC	Glass coverslip	Well-defined microfibers
4:1-1:49 HFIP:MeOH	4-0.1 mg/mL	25 ºC	Silanized Glass	Micro- and nanofibers hierarchically aggregated in doughnut-like supramolecular structures
4:1 HFIP:MeOH	4 mg/mL	25 ºC	AISI 316	Micro- and nanofibers hierarchically aggregated in doughnut-like supramolecular structures
4:1 HFIP:MeOH	4 mg/mL	25 ºC	Plasma-treated polystyrene	Disordered fibre agglomerates
1.9-1:49 HFIP:MeOH	0.5-0.1 mg/mL	25 ºC	Plasma-treated polystyrene	Dendritic-like structures
			N_3-FF-OPrp	
4:1-1:49 HFIP:water	< 1 mg/mL	4 ºC	Glass coverslip	Well-defined spheres of heterogeneous sizes, which aggregate forming honeycomb-like structures

Table 2. For the antiparallel and parallel assemblies formed by three Poc-FF-N_3 strands and optimized at the M06L/6-31G(d), M06L-D3/6-31G(d) and B3LYP-D3/6-31G(d) levels: relative energy (ΔE), average hydrogen bonding parameters, and average π-stacking distances involving the azide and alkyne terminal groups of adjacent molecules.

	ΔE (kcal/mol)	**$d_{H\cdots O}$ (Å), ∠N–H⋯O (º)** [a]	**$d_{N\cdots RC\equiv}$ / $d_{N\cdots HC\equiv}$ (Å)** [b] **$d_{N\cdots N}$ / $d_{C\equiv C\cdots C\equiv C}$ (Å)** [c]
		Poc-FF-N_3	
		B3LYP-D3/6-31G(d)	
Antiparallel	0.0	1.949±0.111, 157.2±8.0	4.564±0.999/4.516±1.370
Parallel	3.7	1.866±0.019, 158.1±8.3	4.809±1.445/3.918±0.108
		M06L-D3/6-31G(d)	
Antiparallel	0.0	2.017±0.158, 154.7±7.2	4.518±0.691/4.192±1.066
Parallel	2.5	1.919±0.063, 153.5±9.4	4.400±0.590/3.911±0.006
		M06L/6-31G(d)	
Antiparallel	0.0	2.007±0.119, 156.7±6.4	4.647±0.974/4.465±1.481
Parallel	0.9	1.930±0.053, 153.4±8.9	4.6857±1.020/3.902±0.044

[a] $d_{H\cdots O}$ and ∠N–H⋯O correspond to the intermolecular (N–)H⋯O distance and the N–H⋯O angle.

[b] For intermolecular azide⋯alkyne interactions in antiparallel β-sheets: $d_{N\cdots RC\equiv}$ and $d_{N\cdots HC\equiv}$ correspond to the distance between the central nitrogen atom of the azide group and each of the two carbon atoms of the alkyne group (RC≡ and HC≡ refer to the internal and external sp-carbon atoms, respectively).

[c] For intermolecular azide⋯azide and alkyne⋯alkyne interactions in parallel β-sheets: $d_{N\cdots N}$ and $d_{C\equiv C\cdots C\equiv C}$ correspond to the distance between the central nitrogen atom of two interacting azide groups and the distance between the geometric centre of two interacting C≡C groups, respectively.

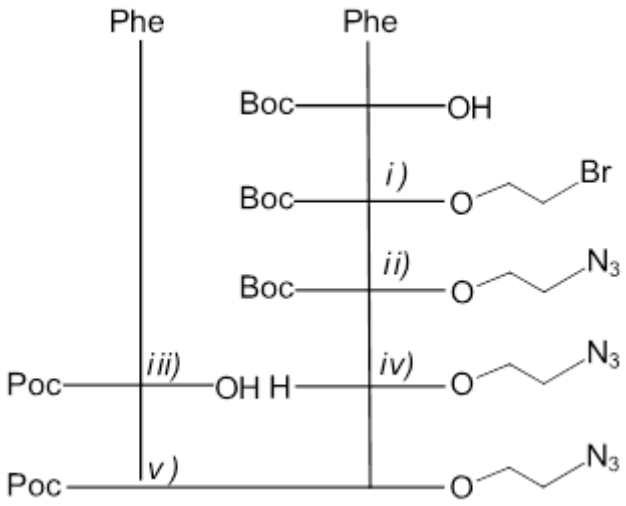

Figure 1

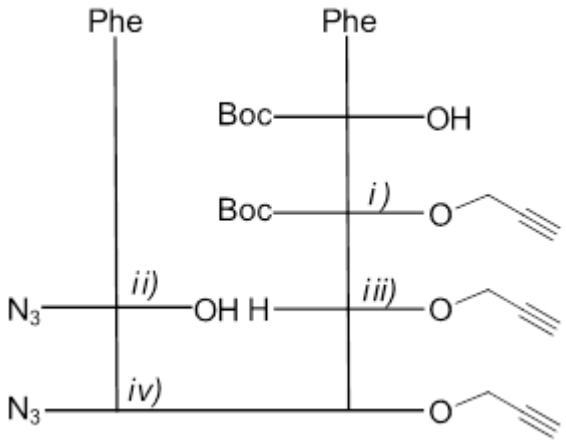

Figure 2

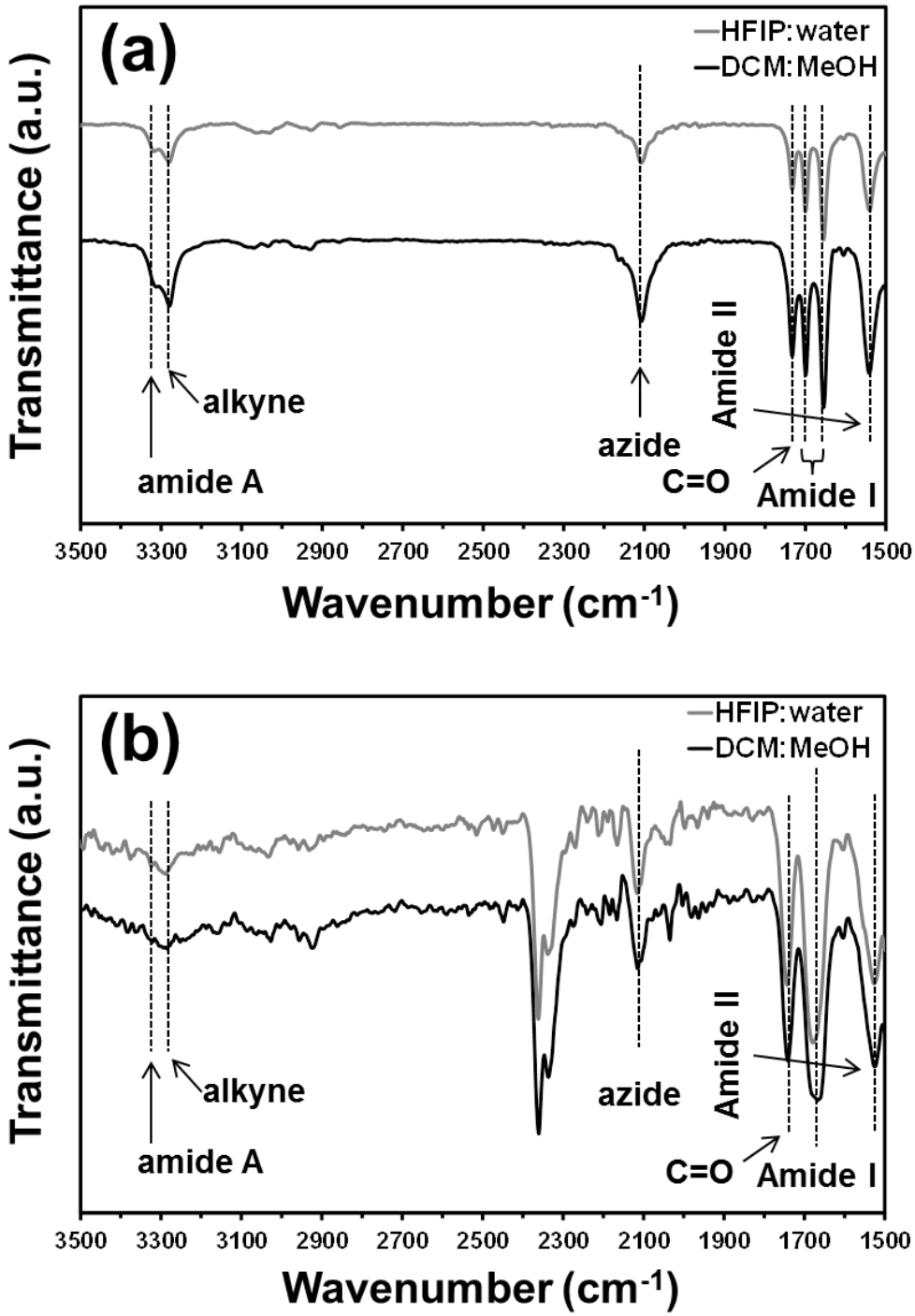
(a)
HFIP:water
DCM:MeOH
Transmittance (a.u.)
alkyne
amide A
azide
Amide II
C=O
Amide I
3500 3300 3100 2900 2700 2500 2300 2100 1900 1700 1500
Wavenumber (cm-1)
(b)
HFIP:water
DCM:MeOH
Transmittance (a.u.)
alkyne
amide A
azide
Amide II
C=O
Amide I
3500 3300 3100 2900 2700 2500 2300 2100 1900 1700 1500
Wavenumber (cm-1)

Figure 3

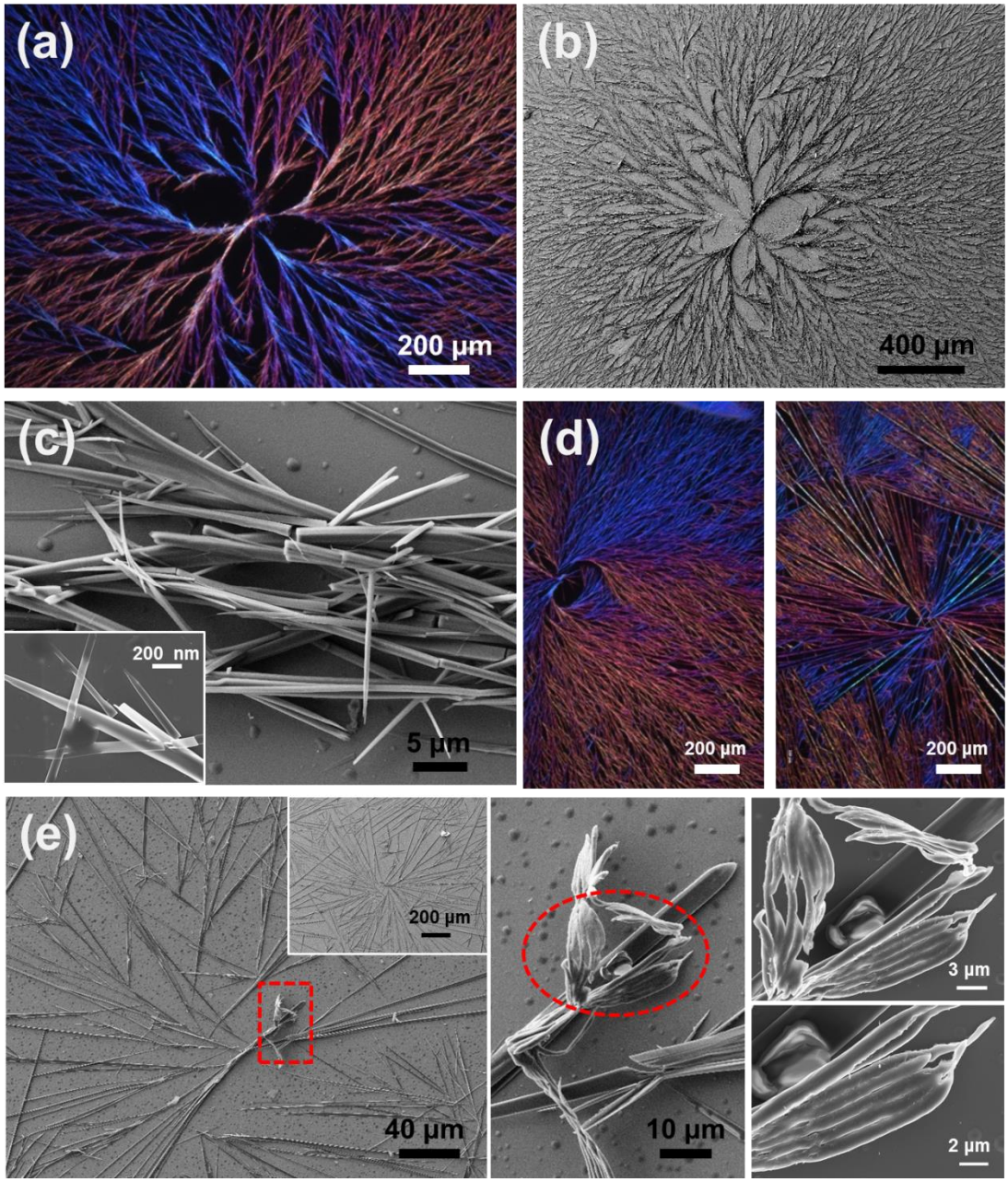
(a)
200 μm
(b)
400 μm
(c)
200 nm
5 μm
(d)
200 μm
200 μm
(e)
200 μm
40 μm
10 μm
3 μm
2 μm

Figure 4

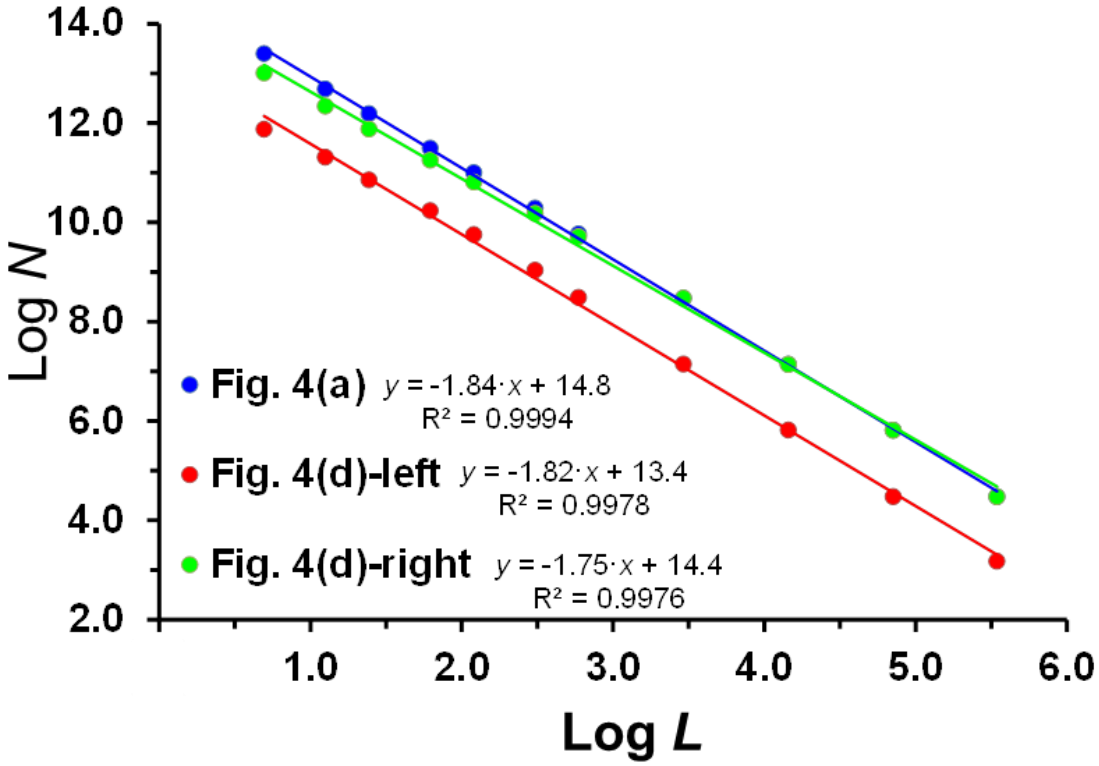
14.0
12.0
10.0
8.0
6.0
4.0
2.0
Log N
1.0
2.0
3.0
4.0
5.0
6.0
Log L
Fig. 4(a) y = -1.84·x + 14.8
R² = 0.9994
Fig. 4(d)-left y = -1.82·x + 13.4
R² = 0.9978
Fig. 4(d)-right y = -1.75·x + 14.4
R² = 0.9976

Figure 5

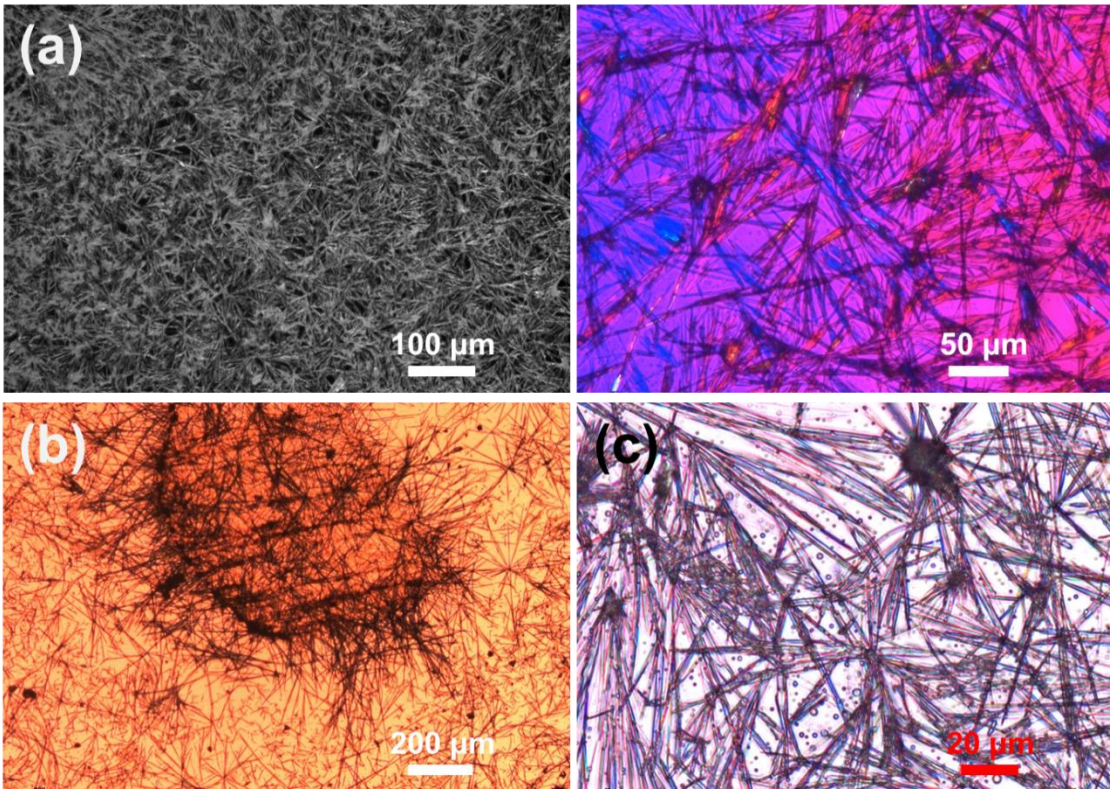

Figure 6

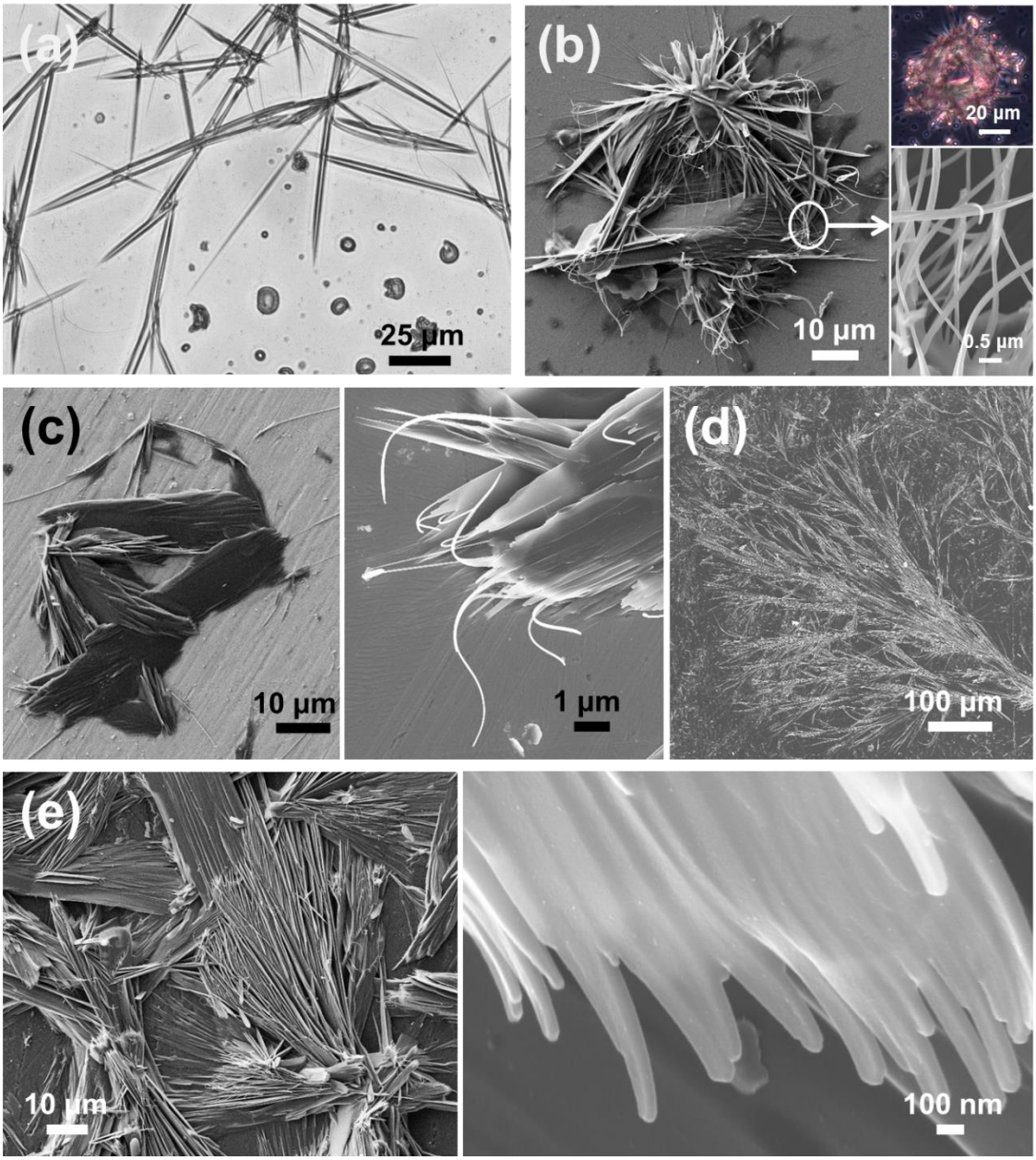

Figure 7

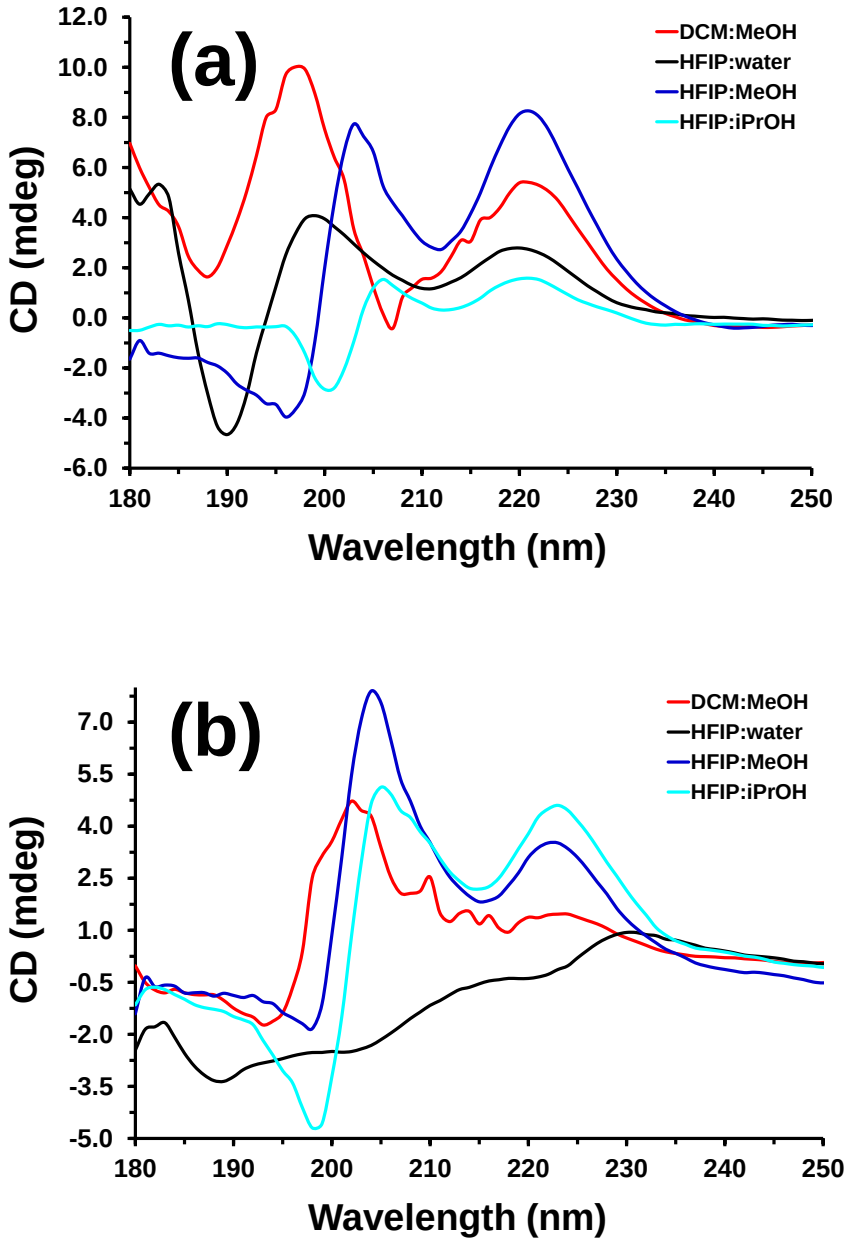
(a)
DCM:MeOH
HFIP:water
HFIP:MeOH
HFIP:iPrOH
CD (mdeg)
12.0
10.0
8.0
6.0
4.0
2.0
0.0
-2.0
-4.0
-6.0
180
190
200
210
220
230
240
250
Wavelength (nm)
(b)
DCM:MeOH
HFIP:water
HFIP:MeOH
HFIP:iPrOH
CD (mdeg)
7.0
5.5
4.0
2.5
1.0
-0.5
-2.0
-3.5
-5.0
180
190
200
210
220
230
240
250
Wavelength (nm)

Figure 8

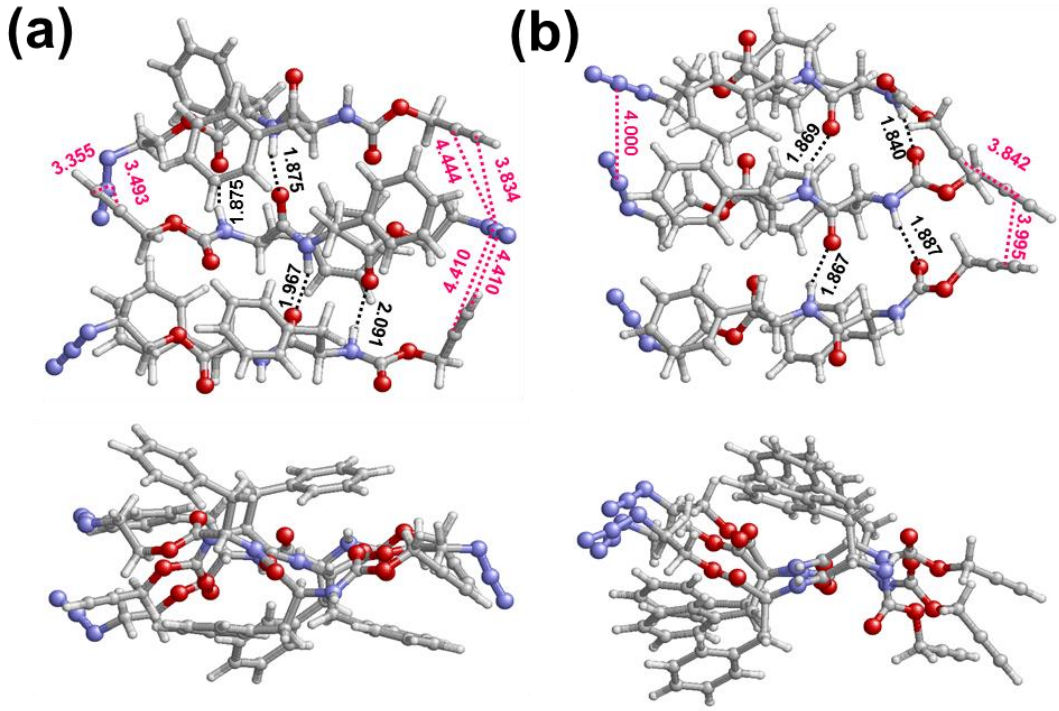
(a)
3.355
3.493
1.875
1.875
4.444
3.834
4.410
4.410
2.091
(b)
4.000
1.869
1.840
3.842
1.887
3.995
1.867

Figure 9

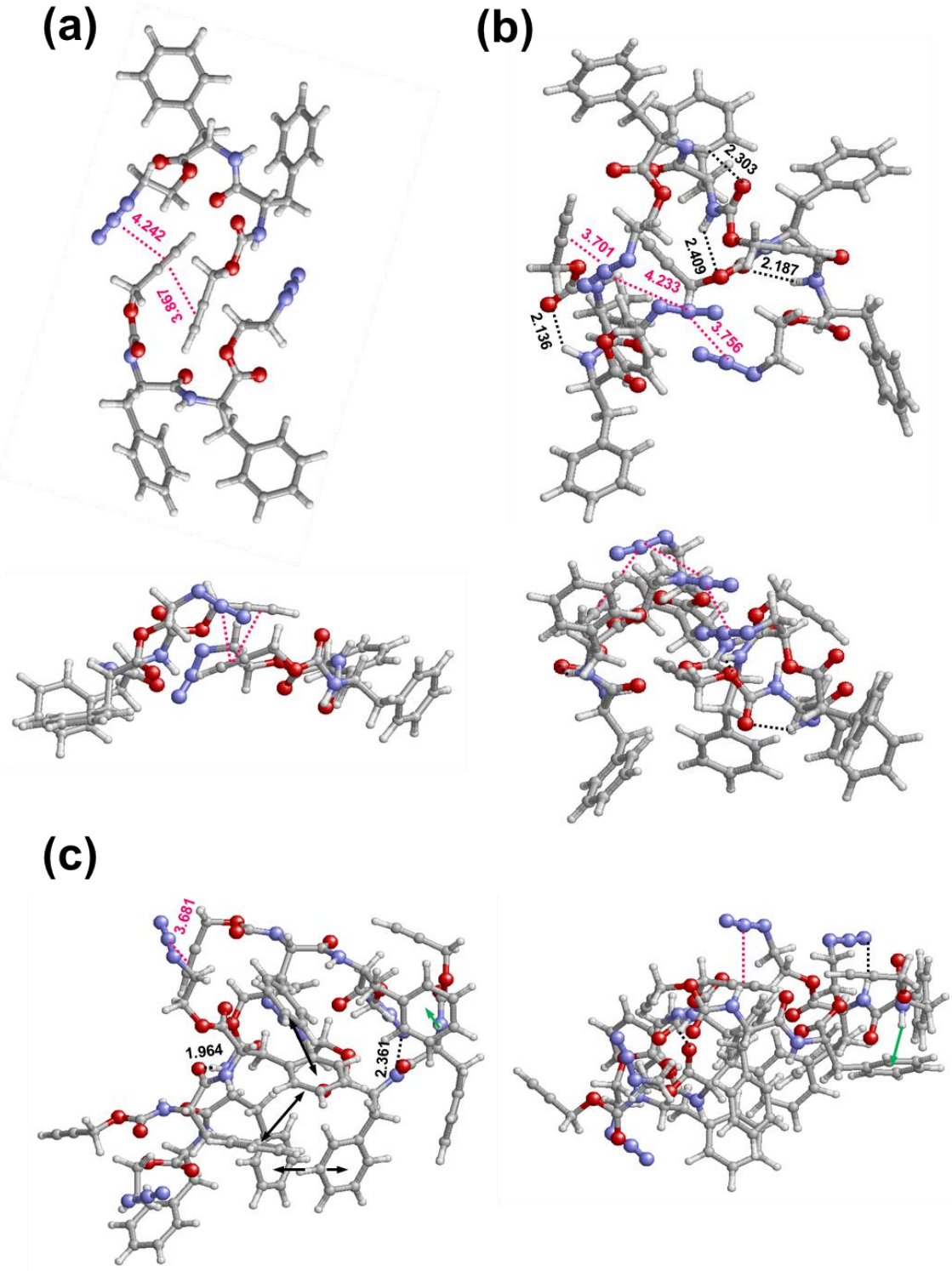
(a)
4.242
3.867
(b)
2.303
3.701
2.409
2.187
4.233
2.136
3.756
(c)
3.681
1.964
2.361

Figure 10

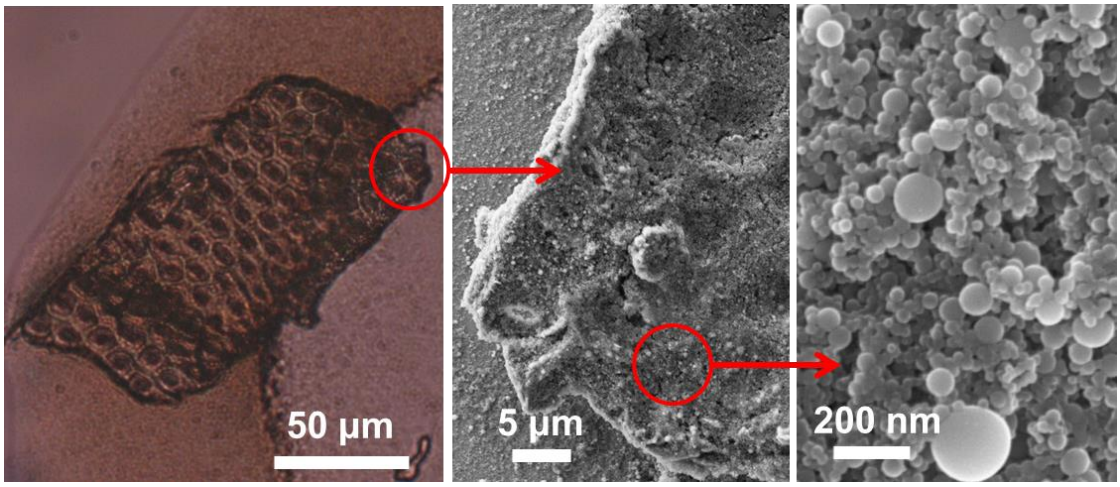

Figure 11

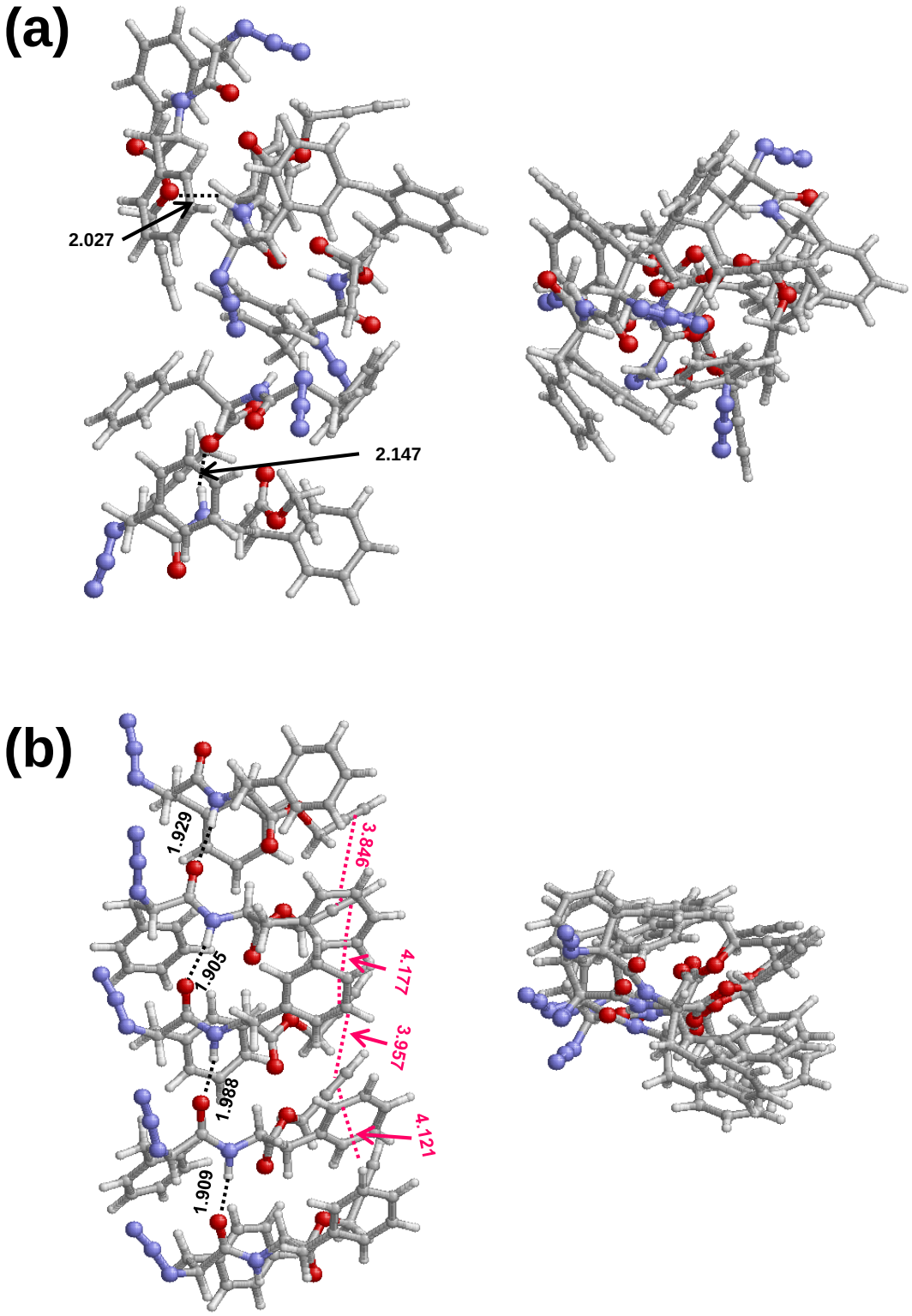

Figure 12

Graphical Abstract

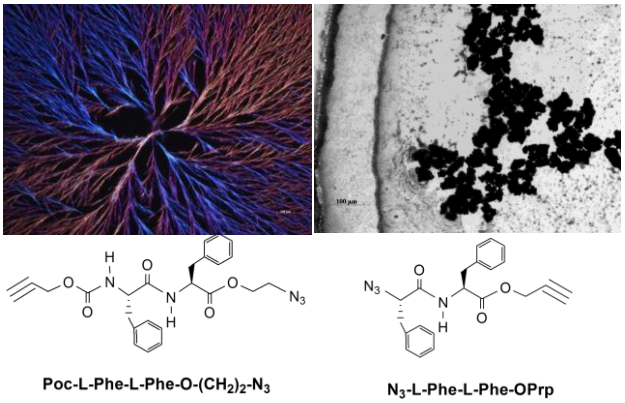

Poc-L-Phe-L-Phe-O-$(CH_2)_2$-N_3

N_3-L-Phe-L-Phe-OPrp